Solar-driven reforming of lignocellulose to H_2 with a CdS/CdO_x photocatalyst

David W. Wakerley†, Moritz F. Kuehnel†, Katherine L. Orchard, Khoa H. Ly, Timothy E. Rosser and Erwin Reisner*

Christian Doppler Laboratory for Sustainable SynGas Chemistry, Department of Chemistry, University of Cambridge, Lensfield Road, Cambridge CB2 1EW, U.K.

†These authors contributed equally to this manuscript.

Summary

Lignocellulose is Earth's most abundant form of biomass and its valorisation to H_2 is a key objective for the generation of renewable fuels. Solar-driven photocatalytic reforming of lignocellulose to H_2 at ambient temperature offers a sustainable route towards this goal, but this reaction is currently limited to noble metal containing systems that operate with low activity under UV light. Here, we report the light-driven photoreforming of cellulose, hemicellulose and lignin to H_2 using semiconducting cadmium sulfide quantum dots in alkaline aqueous solution. We show that basic conditions cause these dots to become coated with oxide/hydroxide *in situ*, presenting a strategy to improve their photocatalytic performance. The system operates under visible light, is stable beyond 6 days and is even able to reform unprocessed lignocellulose, such as wood and paper, under solar irradiation at room temperature, presenting an inexpensive route to drive aqueous proton reduction to H_2 through waste biomass oxidation.

Introduction

As of 2016 the global consumption of fossil-derived oil has reached 1100 barrels (10^5 litres) per second and continues to climb annually.[1,2] Low-cost fuel cannot be produced at this rate indefinitely,[3] and securing and combusting crude oil is causing irreversible environmental damage.[4] Investigations into sustainable alternatives have consequently identified H_2 as a promising energy vector,[5] which can be used directly in an emission-free fuel cell, or as a hydrogenating agent in the

synthesis of renewable liquid fuel.[6] To date however, H_2 is almost exclusively produced through reforming/gasification of fossil-derived coal, gas or oil.[7]

Biomass conversion is one of the most affordable routes to generate sustainable H_2,[8] but this process requires the demanding chemical transformation of lignocellulose. Lignocellulose is the main constituent of biomass and can be cultivated worldwide, even on unfertilised, marginal land.[9] Lignocellulose conversion to H_2 has predominantly been realised through gasification, which uses high temperatures (> 750 °C) to decompose its organic structure and release H_2, alongside other gases, such as CO, CO_2 and CH_4.[10,11] In the interest of increasing the selectivity and efficiency of this conversion, it is possible to replace the thermal input with sunlight. Solar light offers an essentially inexhaustible source of globally available energy and therefore the photoreforming of biomass-derived compounds is a fast growing field of research.[12,13]

Photoreforming requires a photocatalyst able generate holes to oxidise lignocellulose and use the resultant electrons to reduce aqueous protons to H_2.[12] Lignocellulose therefore adopts the role of a hole scavenger, providing a continuous supply of electrons for fuel production. Thus far, this field has focused on H_2 evolution from substrates that could be derived from lignocellulose, such as methanol, glycerol or glucose,[12] but lignocellulose refining is expensive and inefficient, usually requiring acid hydrolysis, enzymatic hydrolysis or pyrolysis to produce more manageable substrates.[12] Viable H_2 production systems must therefore reform lignocellulose directly, to compete with thermochemical processes.[14,15] This is challenging at ambient temperatures, as the structure of lignocellulose has evolved to prevent its consumption by microbial and animal life.[16] Lignocellulose is mainly comprised of cellulose (> 40% in wood stems),[17] a crystalline polysaccharide of anhydroglucose monomers (Fig. 1a). Cellulose is surrounded by branched polysaccharides, called hemicelluloses (20-40%), which are heteropolymers of pentose and hexose sugars. The two cellulosic polymers are further encased in the cross-linked phenolic polymer, lignin (< 35%), and the combined structures form microfibrils that are resistant to chemical transformation.[9] Examples of

the direct photoreformation of lignocellulose or even purified cellulose to H_2 are consequently rare and until now required a UV-light absorbing TiO_2 architecture loaded with expensive, non-scalable noble-metal catalysts, such as Pt and RuO_2.[18–20]

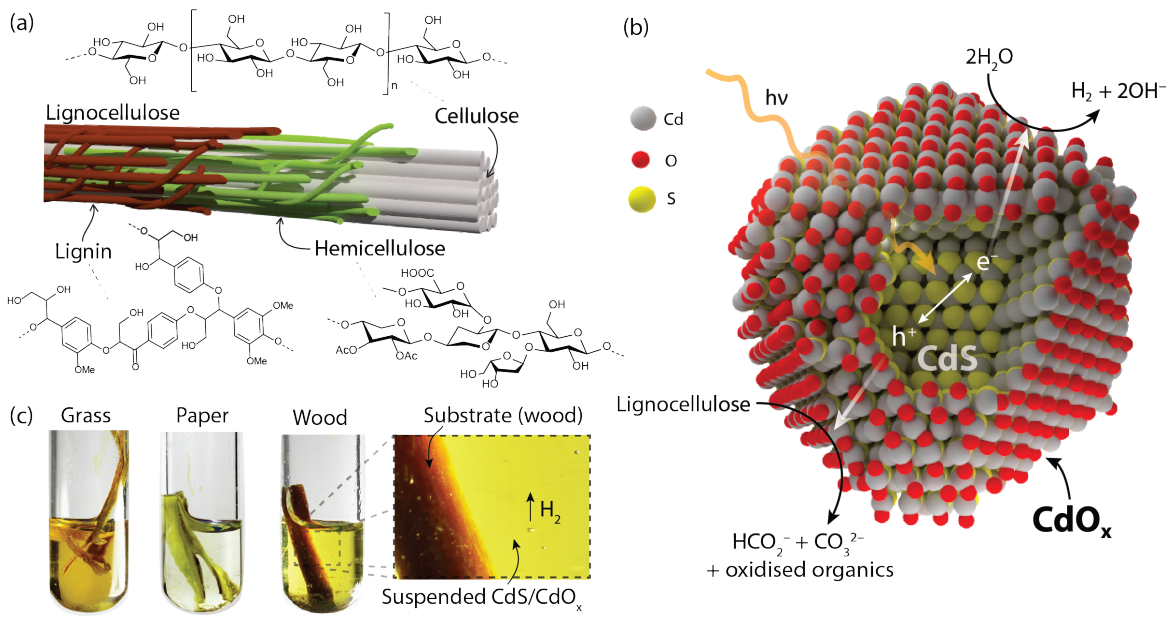

Figure 1 | Photoreforming of lignocellulose to H_2 on CdS/CdO_x. (a) Lignocellulose exists as microfibrils in plant cell walls and is comprised of cellulose surrounded by the less crystalline polymers hemicellulose and lignin.[9,15] **(b)** These components can be photoreformed into H_2 using semiconducting CdS coated with CdO_x (the CdO_x surface is believed to contain some –OH functionality, but H-atoms have been removed in the illustration for clarity). Light absorption by CdS generates electrons and holes, which travel to the CdO_x surface and undertake proton reduction and lignocellulose oxidation, respectively. **(c)** This combination creates a highly robust photocatalyst able to generate H_2 from crude sources of lignocellulose when suspended in alkaline solution and irradiated with sunlight. A video of the photoreforming of paper and wood is provided in Supplementary Video 1.

Herein, we report the development of a photocatalytic system based on semiconducting CdS quantum dots (QDs) able to photoreform cellulose, hemicellulose and lignin into H_2 at room

68 temperature. CdS is an inexpensive, visible-light absorbing photocatalyst with a bulk electronic band
69 gap of around 2.4 eV. The CdS conduction band has a potential of −0.5 V *vs.* the normal hydrogen
70 electrode (NHE),[21] providing sufficient driving force for proton reduction and is responsible for
71 several of the highest reported rates of photocatalytic H_2 evolution.[22] The CdS valence band, at
72 roughly +1.9 V *vs.* NHE, is adequate for saccharide oxidation,[13] but also sufficient for the
73 photooxidation of its constituent sulfide. This photocorrosion has brought the viability of CdS as a
74 sustainable photocatalyst into question, as H_2 evolution has depended on the use of easily-oxidised
75 sacrificial reagents.[23] To circumvent these issues we employ highly alkaline conditions that promote
76 $Cd(OH)_2$/CdO (henceforth CdO_x) formation on the CdS surface (Fig. 1b). The resultant CdS/CdO_x QDs
77 are able to undertake photocatalysis without photocorrosion and light-driven H_2 evolution is
78 achieved through the oxidation of completely unprocessed lignocellulosic substrates (Fig. 1c,
79 Supplementary Video 1). Lignocellulose is also more easily solubilised at high pH[24] and the
80 synergistic interplay between the active photocatalyst formation and the increase in dissolved
81 lignocellulosic substrate produces a system with high rates of H_2 evolution.
82

83 **Characterisation of CdS/CdO_x Quantum Dots**

84 CdS/CdO_x was synthesised from ligand-free CdS QDs with a diameter of *circa* 5 nm,[25] as confirmed by
85 transmission electron microscopy (TEM, Fig. 2a,b). The ligand-free CdS is passivated by weakly-
86 bound tetrafluoroborate anions and *N,N*-dimethylformamide (DMF), presenting an accessible
87 surface that can be modified for improved catalytic activity.[25] Addition of the QDs to basic solution
88 caused CdO_x to instantaneously form on the particle surface through OH^- binding to Cd surface
89 sites.[26] This was confirmed using X-ray photoelectron spectroscopy (XPS) of CdS QDs after
90 suspension in various concentrations of KOH. The expected Cd $3d_{5/2}$ and $3d_{3/2}$ binding energies for
91 emissions in CdS are 405 and 412 eV,[27] respectively, which were observed in the photoemission
92 spectrum of QDs isolated from a pH neutral solution (Fig. 2c, see Supplementary Figure 1 for O and S

spectra). After isolation from 0.1 M KOH the Cd emissions tail towards lower binding energies and after isolation from 10 M KOH the peaks shift 1 eV lower to 404 and 411 eV. The lowered binding energy is consistent with $CdO/Cd(OH)_2$ environments on the CdS surface at high pH.[28] Quantification of CdO_x through analysis of the O-region of the XPS spectrum was not possible due to large quantities of residual KOH, which dominated the spectrum.

Raman measurements provided *in situ* evidence for the formation of surface-bound CdO_x. Under 514 nm laser excitation, highly resolved off-resonant Raman spectra of ligand-free CdS QDs in 0, 0.1 and 10 M KOH aqueous solutions were obtained (Fig. 2d). Vibrational bands at 305 cm^{-1} and 605 cm^{-1} were observed that are assigned to scattering and double-scattering on the longitudinal optical phonon of CdS (LO and 2LO), respectively.[29] As the KOH concentration is increased, a broadening of the LO peak on the low frequency side is observed that cannot be accounted for by the KOH (Fig. 2e and Supplementary Figure 2). Spectral deconvolution by band-fitting analysis revealed contributions from two bands located at 260 cm^{-1} and 292 cm^{-1}. These can be attributed to CdO by comparison to a reference spectrum of CdO (bulk) and literature values.[30,31] The positions of these bands are slightly lower than those reported for bulk CdO (265-268 cm^{-1} and 298-305 cm^{-1}).[31] Although the formation of $Cd(OH)_2$ was not visible in the Raman spectra (see Supplementary Figure 2 for reference spectrum), this does not confirm that the surface consists solely of CdO, as the dynamic nature of the QD modification would introduce numerous Cd–O functionalities.

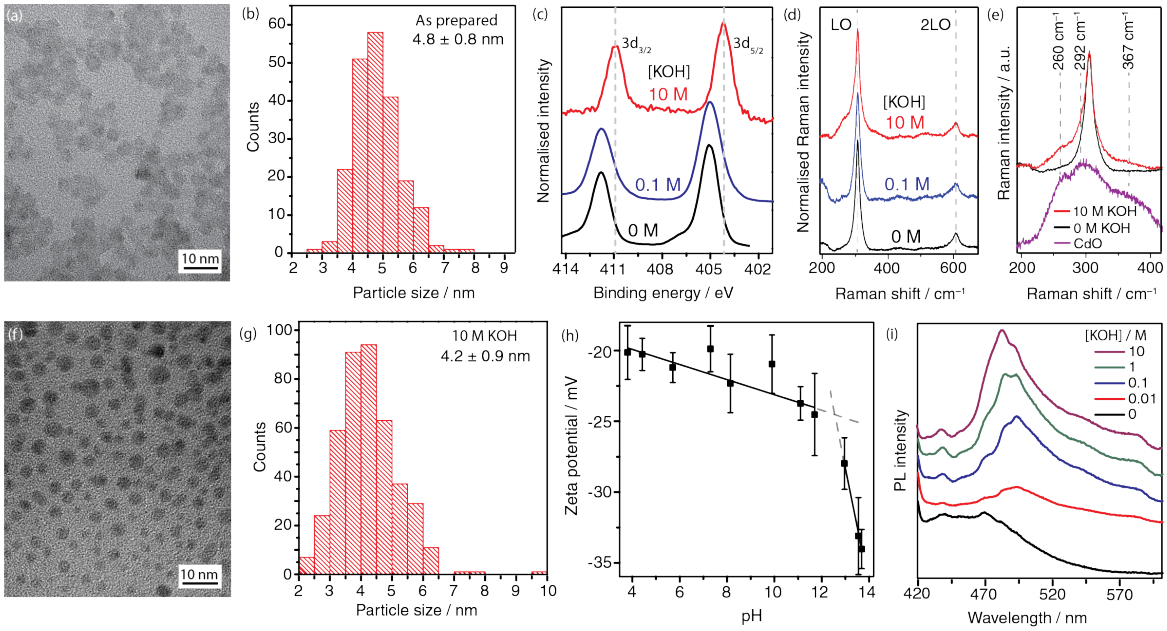

Figure 2 | Characterisation of CdS/CdO$_x$. (a) TEM image of ligand-free CdS QDs and **(b)** corresponding size distribution. **(c)** XPS analysis of the Cd (3d) region of CdS QDs after isolation from aqueous solutions containing various concentrations of KOH. **(d)** Raman spectra of ligand-free CdS QDs with 514 nm excitation at different KOH concentrations. **(e)** Raman spectra of ligand-free CdS in 10 M KOH and in water. In 10 M KOH an interfering spectral signature of CdO can be identified. Reference spectrum of CdO is shown in purple. **(f)** TEM image of CdS/CdO$_x$ after isolation from 10 M KOH and **(g)** corresponding size distribution. **(h)** Zeta potential analysis of a solution of CdS QDs (2 µM) in 0.5 M ionic strength solutions (comprised of HCl, KCl and KOH) at various pH, showing a substantial increase in negative surface charge above pH 12. Error bars represent the standard deviation based on 3 measured samples. Two linear fits are shown; one of the data between pH 12-14 and another below pH 12. **(i)** Photoluminescence emission spectra (excitation/emission bandwidth = 5 nm) at an excitation wavelength of 360 nm of CdS QDs (0.5 µM) in increasingly basic solution.

TEM images of CdS/CdO$_x$ after isolation from 10 M KOH show that the surface change occurs with a concomitant decrease in average particle size by 0.6 nm (Fig. 2f, g). It also causes a change in surface charge as zeta potential analysis of the QDs shows a rapid increase in negative charge above pH 12

130 (Fig. 2h). This shift is similar to that observed on $ZnS/Zn(OH)_2$ surfaces,[32] indicating $Cd–O^-$ is forming
131 on the particle surface. The bulk properties of the particle are unaffected, since the X-ray diffraction
132 pattern displays only marginal changes after dissolution in 10 M KOH (Supplementary Figure 3). The
133 UV-visible spectrum after dissolution in 10 M KOH also retains the light absorption consistent with
134 CdS QDs, although the spectrum is broadened and red-shifted relative to the spectrum in DMF (λ_{max}
135 = 450 nm in DMF and 470 nm in 10 M KOH, Supplementary Figure 4a). This red-shift is attributed to
136 a lower QD dispersibility in aqueous solution, which leads to a degree of particle aggregation similar
137 to that observed previously for ligand-free CdS QDs.[33] We thus propose that CdO_x exists as a
138 monolayer or at most as a few layers on the CdS surface at high concentrations of KOH.

139 The influence of the CdO_x surface passivation on the CdS QD photoluminescence is presented in Fig.
140 2i. As OH^- is added, a stronger near band-gap emission is visible at 480-490 nm, which is most
141 pronounced in 10 M KOH. A comparison between the emission and absorption spectra in 10 M KOH
142 is presented in Supplementary Figure 4b. The increasing intensity of the emission with increasing
143 $[OH^-]$ is attributed to the formation of CdO_x, which acts as a thin surface-passivating shell. It has
144 been shown that similar shells block CdS defect sites that promote radiationless charge-carrier
145 recombination.[26] This fluorescence is not expected to influence the QD photocatalytic activity since
146 the fluorescence quantum yield at the near band-gap emission in 10 M KOH was low (approximately
147 0.05%, Supplementary Figure 4c). The shell is therefore believed to be sufficiently thin to allow
148 tunnelling of electrons and holes from the core-shell interface to the solution.[34]

149

150 **Photoreforming of Cellulose**

151 To test the efficacy of the CdS/CdO_x photocatalyst for lignocellulose reforming, we initially focused
152 on the oxidation of its major component, cellulose. We used the most crystalline and unreactive
153 form, referred to as 'α-cellulose', as its conversion is most crucial if complete lignocellulose
154 reformation is to be achieved. Photocatalysis was carried out with CdS QDs (1 nmol) and α-cellulose

155 suspended in a deaerated aqueous solution (2 mL) kept at 25 °C, which was irradiated with
156 simulated solar light (AM 1.5G, 100 mW cm^{-2}). The cellulose exists as a suspension due to its low
157 solubility and optimisation revealed that a loading of 50 mg mL^{-1} led to the highest photocatalytic
158 activity (Supplementary Table 1). Large volumes of H_2 could be produced provided strongly alkaline
159 conditions were employed (Fig. 3a) with the activity rapidly increasing towards 10 M KOH. This
160 concurs with the *in situ* formation of CdO_x on the QD surface (Fig. 2) and a similar pH dependence
161 was observed when photoreforming other substrates (Supplementary Table 2), as seen in previous
162 CdS-based systems.[35] H_2 evolution by the photocatalyst originates mostly from reduction of aqueous
163 protons, as photocatalysis in D_2O produced D_2 and HD in a 4:1 ratio (Supplementary Figure 5).
164 Formation of the latter originates from H/D exchange with cellulose OH groups. No H_2 was detected
165 without QDs or light (Supplementary Table 1).

166 The high concentration of KOH provides the added benefit of solubilising a portion of the suspended
167 cellulose, as known for aqueous NaOH.[24] Dissolved cellulose chains were confirmed to be the major
168 substrate through use of a 10 M KOH solution that had been stirred in the presence of α-cellulose for
169 24 hours and subsequently centrifuged to remove the suspended, insoluble cellulose. The
170 supernatant was then added to CdS/CdO_x QDs and irradiated (Supplementary Figure 6,
171 Supplementary Table 3). H_2 evolution from this solution was initially faster relative to the rate
172 observed when using suspended cellulose, as more dissolved substrate was available. Without the
173 suspended cellulose present however, the activity dropped over time as the solubilised substrate
174 depleted. The photoreforming reaction therefore occurs through continuous dissolution of the
175 suspended cellulose by the basic solution, followed by its fast oxidation by the CdS/CdO_x
176 photocatalyst.

177 Long-term photocatalytic H_2 evolution from cellulose is illustrated in Fig. 3b. After 6 days there was
178 no evidence of photocorrosion and nearly 600 $mmol_{H_2}\ g_{CdS}^{-1}$ had been produced in the headspace of
179 a closed photoreactor. The activity of CdS/CdO_x is over an order of magnitude higher than the

aforementioned TiO_2 systems, even without the use of expensive noble metal co-catalysts or UV light. No evolution of CO was observed during catalysis (CO detection limit = 35 ppm), resulting in H_2 free of fuel-cell inhibitors. All CO_2 generated was sequestered by the basic solution as CO_3^{2-} (see discussion of Fig. 3c), removing any potential environmental impact of the oxidation reaction. CdS/CdO_x without cellulose present (Fig. 3b, black line) shows 10% of the H_2 evolution activity for the first 24 hours and then ceases (4% after 6 days), which originates from oxidation of residual DMF from the QD stock solution. The narrower bandgap of CdS also allows the system to function effectively under visible light and 50% of the catalytic activity was maintained by CdS/CdO_x when UV-light (λ < 400 nm) was filtered from the solar spectrum (Supplementary Table 1). The drop in activity is due to the decrease in the number of photons, demonstrating that UV-light is not needed to facilitate the photoreforming reaction.

An external quantum yield of 1.2 ± 0.4 % was achieved when irradiating with 430 nm monochromatic light (Supplementary Table 4), which is comparable to reported efficiencies of Pt/TiO_2 for the much simpler glucose reforming reaction under UV-light.[36] The yield was substantially higher when photoreforming MeOH (17.7 ± 1.5 %, Supplementary Table 5), indicating that the efficiency is reduced by the slow oxidation rate of the polysaccharide chains, as well as light-scattering by the cellulose suspension.

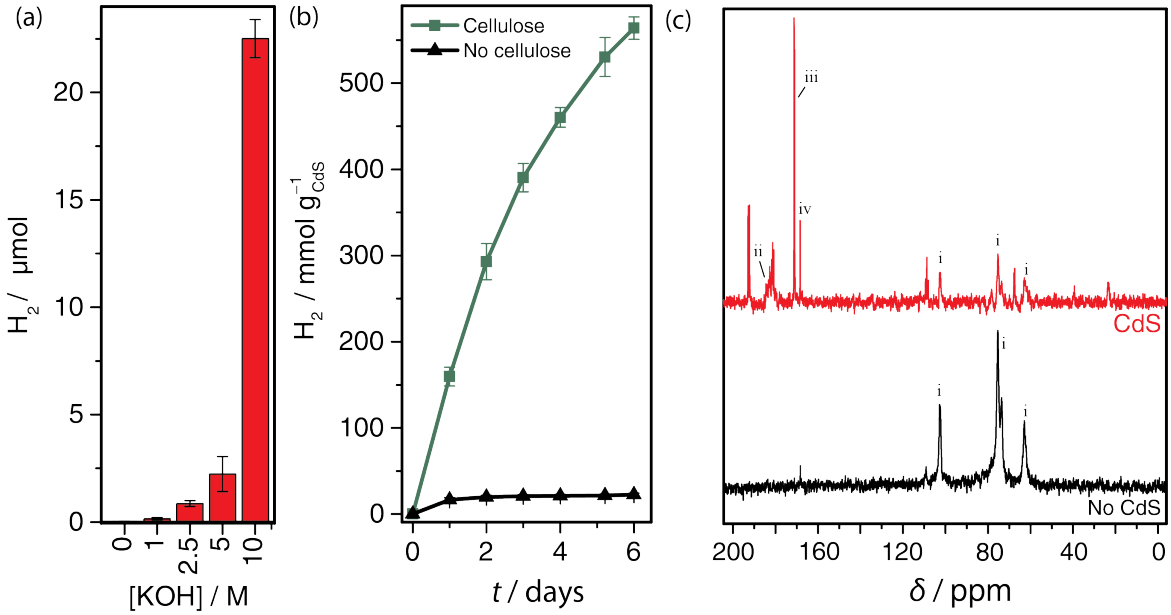

Figure 3 | Photoreforming of cellulose to H_2 using CdS/CdO_x. (a) The pH dependence of the photocatalytic H_2 evolution from a 2 mL aqueous solution of ligand-free CdS QDs (0.5 μM) with 50 mg mL^{-1} α-cellulose after 18 hours of irradiation. **(b)** Long-term photocatalytic cumulative production of H_2 by CdS/CdO_x QDs (0.5 μM) with and without 50 mg mL^{-1} α-cellulose in 2 mL KOH (10 M). The line between data points has been added to guide the eye. **(c)** ^{13}C-NMR spectra of the supernatant from a suspension of uniformly ^{13}C-labelled cellulose (10 mg) in 10 M NaOD in D_2O (1 mL) after 3 days of irradiation with and without 1 nmol of CdS/CdO_x QDs. Photocatalysis was carried out with simulated solar light (AM 1.5G, 100 mW cm^{-2}) under an anaerobic atmosphere at 25 °C. Error bars represent the standard deviation based on 3 measured samples.

The products of α-cellulose oxidation were identified by ^{13}C-NMR spectroscopy using uniformly ^{13}C-labelled cellulose in 10 M NaOD in D_2O (Fig. 3c). Photocatalysis was carried out with 10 mg of ^{13}C α-cellulose in NaOD for 3 days, after which the reaction solution was filtered of insoluble cellulose and analysed. A control experiment wherein ^{13}C-cellulose was irradiated without CdS/CdO_x produced signals between δ = 55-110 ppm (Fig. 3c, black line, i), corresponding to C-environments in the

anhydroglucose repeating unit.[37] This confirms that the basic conditions are able to partially dissolve the α-cellulose, providing solvated cellulose as a substrate for photocatalysis.

After irradiation in the presence of CdS/CdO_x the polymeric cellulose resonances (δ = 55-110 ppm, i) are still present, alongside a broad polymeric carboxylic acid resonance (δ = 182 ppm, ii), from oxidised polysaccharide end groups.[38] Decomposition of the cellulose by CdS/CdO_x forms smaller saccharides, however sharp, monosaccharide peaks are not present in the spectrum. This suggests that if smaller saccharides do form they are rapidly consumed by the photocatalyst. The fast affinity of the photocatalyst for smaller saccharide oxidation was confirmed by photoreforming 0.1 M glucose, which produced H_2 at a rate of 10.0 $mmol_{H_2}\ g_{CdS}^{-1}\ h^{-1}$ (Supplementary Table 2); 130% higher than with α-cellulose (4.4 $mmol_{H_2}\ g_{CdS}^{-1}\ h^{-1}$). In Pt/TiO_2 systems dehydration of monosaccharides produces intermediate furfural species, such as 5-hydroxymethyl furfural (HMF),[20] however HMF resonances are not visible in the ^{13}C-NMR spectrum after photocatalysis, (reference spectrum provided in Supplementary Figure 7d). This illustrates that either HMF is not formed or that upon its formation it is rapidly decomposed. The latter is unlikely as photoreforming HMF by the photocatalyst proceeded at a relatively slow rate of 4.7 $mmol_{H_2}\ g_{CdS}^{-1}\ h^{-1}$ (Supplementary Table 2). Instead, formate was identified as the major intermediate (δ = 171 ppm, iii), which is a product of biomass oxidation by thermally-driven metal oxide catalysts.[39] The accumulation of formate was assigned to its slow oxidation by CdS/CdO_x, as its photoreformation generated H_2 at an even slower rate of 1.3 $mmol_{H_2}\ g_{CdS}^{-1}\ h^{-1}$ (Supplementary Table 2). A combination of decarboxylation of carboxylic acids and formate oxidation then produces CO_2, which was solubilised as carbonate (CO_3^{2-}) at the employed pH (δ = 169 ppm, iv) (Fig. 3c). These assignments were corroborated by reference to authentic samples and ^{1}H-NMR spectroscopy (Supplementary Figure 7).

^{13}C-NMR spectroscopy was also undertaken of insoluble cellulose that had been irradiated for 12 hours in 10 M $NaOD/D_2O$ both with and without CdS/CdO_x. The suspended cellulose was collected

after photocatalysis *via* centrifugation and dissolved in molten $ZnCl_2$ before measuring a spectrum (Supplementary Figure 7e).[40] Both spectra showed the expected cellulose resonances, as well as numerous sp^2 C-environments. When CdS/CdO_x is present there are a number of extra peaks that were assigned to the heterogeneous oxidation of the cellulose. This indicates that there is both homogeneous and heterogeneous oxidation of the cellulose chains during photocatalysis, however due to the mass-transport limitations of the heterogeneous reaction, oxidation of the dissolved cellulose will provide the major contribution to the H_2 evolution activity.

Proton reduction is expected to occur on Cd chalcogenides through Cd^0 sites formed by electron accumulation on the photocatalyst surface,[41] but this leads to slow rates of H_2 evolution. Transition metal co-catalysts are thus added to accelerate the proton reduction activity, but showed a limited effect when oxidising cellulose. Addition of $Ni(BF_4)_2$ lowered the H_2 generated and K_2PtCl_4 halted activity completely over 24 hours of photocatalysis (Supplementary Table 6). Addition of $Co(BF_4)_2$ resulted in a limited increase in the H_2 produced (12%), but only after several days of photocatalysis (Supplementary Figure 8). XPS analysis of $Co(BF_4)_2$ in 10 M KOH showed emissions consistent with $Co(OH)_2$/Co(O)OH (Supplementary Figure 9),[42] which is believed to be the co-catalyst in this case. When replacing cellulose with more easily-oxidised glucose the addition of Co ions had a larger influence on the photoactivity, increasing the H_2 generated by over 100% (Supplementary Table 2). The addition of the Co co-catalyst does not have a large influence when cellulose reforming as the cellulose oxidation reaction limits the rate of photocatalytic H_2 generation on CdS/CdO_x.[43]

This was further confirmed through studies of the kinetic isotope effect in a solution of H_2O/NaOH *vs.* D_2O/NaOD. When the rate of reaction is dictated by breaking/making a H-containing bond the activity drops substantially upon changing to deuterated substrates, due to the lower vibrational frequency of the D-containing bond. In the deuterated solvent, the rate of photocatalysis was lowered by only 25% (k_H/k_D of 1.35 ± 0.16) (Supplementary Table 7), indicating that the formation/cleavage of an H–H/O–H bond is not rate-limiting. The limiting oxidation rate is reflected

262 in the conversion yield of cellulose to H_2, which reached a maximum of 9.7% after 6 days
263 (Supplementary Table 8, this data was corrected by background activity and assumes a theoretical
264 maximum of 12 equivalents of H_2 form per anhydroglucose monomer).[18] The relatively low yield is
265 not yet competitive with the conversion attained by thermochemical reforming processes[12] due to
266 the inaccessibility of the undissolved cellulose.

267 **Photoreforming of Lignocellulose**

268 Study into the reformation of the other lignocellulose components, lignin and hemicellulose, is
269 presented in Fig. 4a, which shows the H_2 evolved per weight of added CdS and $Co(BF_4)_2$ co-catalyst
270 (Supplementary Table 9). Hemicellulose (xylan from beech wood) could be reformed at similar rates
271 to α-cellulose, as expected from its similar chemical composition. A lowered loading of hemicellulose
272 at 25 mg mL^{-1} was used to reflect the levels of hemicellulose present in lignocellulose. The
273 heightened specific H_2 evolution is due to the higher solubility of hemicellulose, which presents
274 more accessible oxidation sites for the particulate CdS/CdO_x photocatalyst.

275 Lignin is strongly light-absorbing and consequently its light-driven oxidation to form H_2 has rarely
276 been reported.[44,45] UV-visible spectroscopy of lignin shows a broad absorption peaking at 300 nm
277 with a shoulder at 350 nm that tails into visible wavelengths of light, the region over which wide-
278 band gap semiconductors absorb most strongly. The smaller band gap of CdS/CdO_x absorbs
279 wavelengths above 420 nm, where there is little competition for light between the photocatalyst
280 and substrate (Supplementary Figure 10), allowing photocatalysis to occur effectively. At lignin
281 loadings of 0.25 mg mL^{-1}, CdS/CdO_x was able to evolve H_2 at a rate of 0.26 $mmol_{H_2}\ g_{cat.}^{-1}\ h^{-1}$ (Fig. 4a).
282 The decomposition of lignin during photocatalysis was followed by UV-visible spectroscopy over 5
283 days of irradiation, which showed a decrease in the peak at 300 nm and growth of the shoulder at
284 350 nm (Supplementary Figure 11a). This change is a result of oxidation of phenols within lignin to
285 quinones.[46] This also occurred without CdS/CdO_x present, due to UV-light absorption and self-
286 oxidation by lignin, but 3.7 times slower with no evolved H_2 (Supplementary Figure 11b/c).

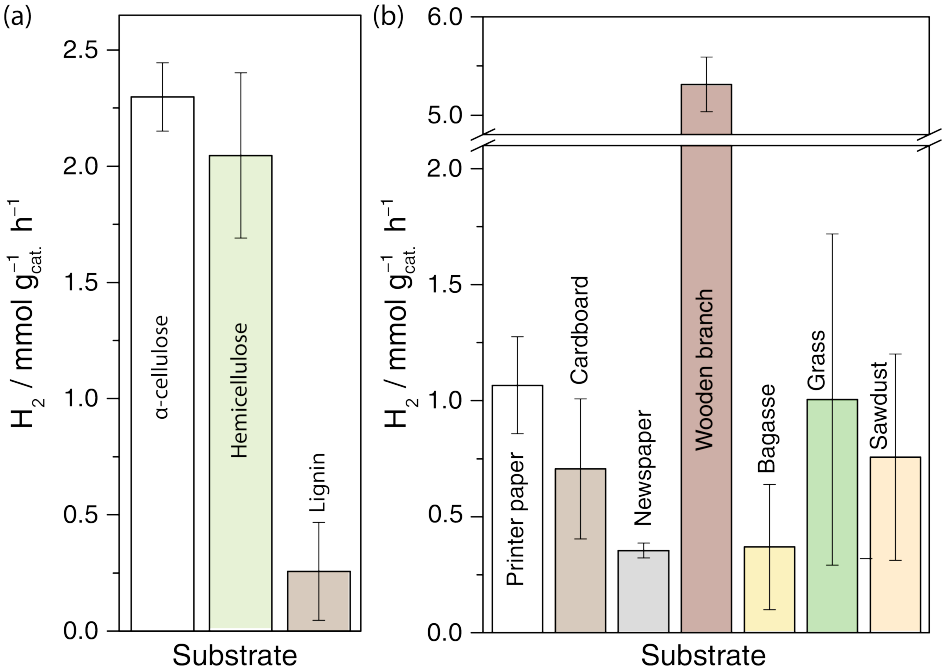

Figure 4 | The rate of H_2 generation through photoreforming lignocellulose on CdS/CdO_x. Photocatalytic production of H_2 (AM 1.5G, 100 mW cm^{-2}) over 24 hours with CdS/CdO_x QDs (0.5 μM) and $Co(BF_4)_2$ (0.34 mM) in 2 mL KOH (10 M, 25 °C, anaerobic atmosphere) with **(a)** 50 mg α-cellulose mL^{-1}, 25 mg hemicellulose (xylan from beech wood) mL^{-1} and 0.25 mg lignin mL^{-1}, and **(b)** 50 mg mL^{-1} of raw and waste biomass substrates. All values are background corrected by the activity without substrate. Error bars represent the standard deviation based on 3 measured samples.

Solar-driven H_2 evolution from unprocessed lignocellulose stands as a long-sought objective for progress in the field of biomass conversion.[12] Fig. 4b (Supplementary Table 10) summarises the rate of H_2 evolution from suspensions of raw biomass available in areas local to Cambridge, UK and lignocellulosic waste by CdS/CdO_x with $Co(BF_4)_2$ co-catalyst. Each source was added to the reaction mixture after a rough cutting procedure to obtain pieces < 0.25 cm long and the H_2 produced was measured after 24 hours of solar irradiation. Rates of over 5 $mmol_{H_2}$ $g_{cat.}^{-1}$ h^{-1} were observed using

302 wood from a tree branch, whereas the other natural lignocellulose sources (bagasse, sawdust and
303 grass) exhibited lower activity. Waste paper, cardboard and newspaper were also reformed to H_2,
304 despite the highly crystalline cellulose present in their structure. The rate at which H_2 is evolved from
305 each substrate competes with the activity of purified monosaccharide reforming systems (typically 1
306 to 9 $mmol_{H_2}\ g_{cat.}^{-1}\ h^{-1}$)[12] and is two orders of magnitude higher than previous reports of
307 photocatalytic lignocellulose reforming.[20] The high activity is assigned to the employed conditions
308 that benefit both the photocatalyst and the substrate; the alkaline conditions provides an *in situ*
309 pretreatment of the lignocellulose, dissolving hemicellulose, lignin, cellulose and other saccharides
310 into solution[47] and also facilitate CdO_x deposition on the CdS, creating a photocatalyst that is active
311 and robust against corrosion. This provides a one-pot system that is responsive to highly
312 unprocessed substrates, allowing H_2 generation from the most ubiquitous lignocellulose in a given
313 area. It should be noted that unreacted biomass remains after 24 hours due to incomplete substrate
314 conversion.

315

316 **Mechanism of Lignocellulose Reforming on CdS/CdO_x**

317 Photocatalytic lignocellulose oxidation is often believed to occur through the formation of hydroxyl
318 radicals (·OH), which subsequently oxidise the substrate.[20] This possibility was explored using the
319 ·OH-scavenger benzene-1,4-dicarboxylic acid (terephthalic acid, TPA). TPA reacts with ·OH to form 2-
320 hydroxyterephthalic acid (TPA-OH), which can be characterised by its fluorescence at 430 nm when
321 excited with 315 nm light.[48] CdS QDs irradiated for 18 hours in the presence of TPA showed low
322 levels of TPA-OH formation below pH 14 (Supplementary Figure 12a), typically amounting to < 2
323 µmol ·OH when compared to a TPA-OH reference (assuming the reaction yield of ·OH and TPA to be
324 35%,[48] Supplementary Figure 12b). Above pH 14, when CdS/CdO_x is formed, no TPA-OH was
325 detected and therefore it is unlikely that ·OH plays a dominant role in the presented system.

326 Function of the probe above and below pH 14 was confirmed through controlled generation of ·OH
327 by H_2O_2 photolysis (Supplementary Figure 13).[49]

328 Instead, we propose that the CdO_x coverage promotes effective binding between photocatalyst and
329 the substrate, which would contain numerous alkoxide groups at the employed pH. This interaction
330 may be similar to TiO_2, which forms Ti–O–R bonds during photocatalysis, facilitating hole transfer
331 and weakening C–C bonds, leading to efficient oxidation to CO_2.[50] Lignocellulosic substrates may
332 bind to the CdS/CdO_x surface through analogous Cd–O–R bonds, as evidenced by the formation of
333 the decarboxylation product, CO_3^{2-}. Such binding is not normally possible on CdS QDs as available
334 Cd-binding sites are passivated by surface ligands[25] or sulfide. We therefore speculate that dissolved
335 lignocellulose chains bind to the CdS/CdO_x surface, allowing the photocatalyst to undertake fast
336 oxidation of alcohols to aldehydes. At this point, C–C bond cleavage can generate formate, or the
337 aldehyde can be further oxidised to a carboxylic acid, which is decarboxylated to CO_3^{2-}.

338 This reaction almost completely occurs in the homogeneous phase using solubilised lignocellulosic
339 biomass, although a small amount of photoreforming on the surface of insoluble substrates may
340 occur based on ^{13}C-NMR evidence (Supplementary Figure 7e). A strong interaction between the CdO_x
341 surface and insoluble cellulose is also apparent in TEM images after reforming, which show the
342 particles embedded in a cellulose matrix (Supplementary Figure 14).

343 **Conclusions**

344 We have presented a route to valorise unprocessed lignocellulose to H_2 at room temperature using
345 visible light and CdS/CdO_x quantum dots. This photocatalyst undertakes biomass oxidation, which
346 provides electrons for the reduction of aqueous protons to generate H_2. High rates of H_2 evolution
347 were achieved, without CdS photocorrosion or noble metal co-catalysts, through use of highly basic
348 conditions that synergistically enabled formation of robust CdS/CdO_x and dissolution of
349 lignocellulose. The oxidation reaction generates CO_2 that is sequestered as carbonate, which leads to
350 an overall negative CO_2 balance in the atmosphere when taking into account the CO_2 fixation
351 required for biomass growth. The system's tolerance to a range of substrates is particularly
352 appealing for H_2 generation without need for lignocellulose processing. Future development should
353 now focus on replacing the Cd with a more environmentally benign metal.

354

355 **Methods**

356 **Reagents.** α-cellulose, hemicellulose (xylan from beechwood), lignin (alkali), CdO and $CdSO_4$ were
357 obtained from Sigma Aldrich and used without further purification. Semiconductor-grade KOH
358 (Sigma Aldrich, 99.99%) was used to ensure impurities were not present during photocatalysis.
359 Cobalt(II) tetrafluoroborate hydrate, 96% (assumed to be $Co(BF_4)_2{\cdot}6H_2O$) was purchased from Alfa
360 Aesar. NaOD (40 %wt in D_2O, 99% atom% D) and D_2 (99.8% atom D) were purchased from Sigma-
361 Aldrich. ^{13}C cellulose was purchased from IsoLife. Wood from the branch of a London plane tree was
362 obtained from a tree on Lensfield Road, Cambridge, UK. Sawdust was obtained from a local sawmill
363 (B&Q, Cambridge) and grass was attained from a garden in North Cambridge. Cardboard was
364 obtained from a Sigma Aldrich box, newspaper from an issue of the Cambridge News, bagasse from
365 a Duni bagasse plate and paper from Office Depot. Waste cellulose and biomass sources were cut

366 roughly into pieces < 0.25 cm long before use. All other reagents were obtained from commercial
367 sources at the highest available purity.

368 **Equipment.** UV−Visible spectra were recorded on a Varian Cary 50 UV−Vis spectrophotometer. ^{1}H
369 and ^{13}C-NMR spectra were recorded on a Bruker 400 MHz Avance spectrometer at room
370 temperature. Transmission electron microscopy (TEM) images were collected using a FEI Philips
371 Tecnai 20 microscope with 200 kV accelerating voltage. XPS analysis was carried out at the
372 Cambridge Microelectronics centre on a Thermo Scientific ESCALAB Xi^{+} XPS Microprobe in an
373 ultrahigh vacuum chamber. Freeze drying was carried out in a VirTis SP Scientific freeze dryer.
374 Powder X-ray diffraction measurements were carried out on an X'Pert PRO diffractometer
375 (PANalytical BV). Photoluminescence measurements were carried out on an Edinburgh Instruments
376 FS5 spectrofluorometer using a 395 nm long-pass filter to remove scattered light where necessary.
377 pH was measured on a Mettler Toledo pH meter and probe, with the exception of the pH of
378 solutions containing [KOH] > 1 M, which was estimated based on the assumption $[OH^{-}] \approx$ [KOH].

379 **Synthesis of oleic acid capped CdS quantum dots (CdS-OA)**. CdS-OA were synthesised following a
380 modified literature procedure.[51] A mixture of CdO (0.64 g) and oleic acid (OA, 29 mL) in octadecene
381 (89 mL) were heated under an Ar atmosphere to 280 °C. Separately, a solution of sulfur (0.08 g) in
382 octadecene (20 mL) was prepared. Half of the sulfur solution was then added rapidly to the Cd-
383 containing solution and the other half was added continuously over the course of 2 minutes. The
384 vessel was then immediately cooled to 220 °C with N_2 gas and rapidly cooled in a water bath. The
385 solution was diluted with 1:1 hexane:methanol (100 mL) and the particles were precipitated using
386 excess acetone (*c.a.* 300 mL). Isolation of the particles was achieved by centrifugation at 5000 rpm
387 for 3 min, after which they were re-dispersed in hexane. Two further washing steps were carried out
388 by dispersion in hexane and precipitation with acetone, before finally dispersing in hexane.

389 **Ligand-free CdS quantum dots (CdS-BF_4)**. Ligand-free CdS QDs were synthesised following a
390 reported literature procedure.[25] A solution of CdS-OA in hexane (3 mL) was reduced to dryness and

391 re-dispersed in a mixture of anhydrous $CHCl_3$ (15 mL) and anhydrous *N,N*-dimethylformamide (DMF,
392 1.9 mL) under a N_2 atmosphere. Et_3OBF_4 (1.0 M in dichloromethane, 9 mL) was added and the
393 reaction solution was stirred for 1 hour. Me_3OBF_4 (1.0 M in acetonitrile) was added slowly until the
394 particles precipitated (*c.a.* 3 mL). The precipitate was collected by centrifugation (6000 rpm, 3 min),
395 and re-dispersed in a minimum of DMF. The QD concentration and particle size was determined by
396 UV-visible spectroscopy based on the position and size of the absorption maximum around 440-450
397 nm in DMF.[52] All experiments using CdS-BF_4 in aqueous solution were prepared by first removing the
398 DMF *in vacuo* while stirring.

399 **Photocatalytic generation of H_2.** Photocatalysis was carried out in a Pyrex glass photoreactor
400 thermostated at 25 °C. Solar irradiation was emulated by a solar light simulator (Newport Oriel, 100
401 mW cm^{-2}) equipped with an air mass 1.5 global filter (AM 1.5G) with a water filter (10 cm path
402 length) to remove IR radiation. In a typical experiment ligand-free CdS QDs in DMF (1 nmol) were
403 transferred to a photoreactor and the DMF was removed *in vacuo* while stirring. Upon removal of
404 the solvent, the substrate and 2 mL of 10 M KOH were added. Co-catalyst solutions were made
405 through dissolution of the metal salt in 10 M KOH and were added to the reaction solution when
406 required. The photoreactor was sealed with a rubber septum and purged with N_2 (containing 2% CH_4
407 for gas chromatographic analysis, see below) for 10 min, after which the vial was irradiated whilst
408 stirring at 600 rpm. The accumulation of H_2 was quantified through periodic headspace gas analysis
409 (50 µL) by gas chromatography.

410 **Gas analysis.** Gas chromatography (GC) was carried out on an Agilent 7890A gas chromatograph
411 with a thermal conductivity detector. H_2/D_2 were analysed using a HP-5 molecular sieve column
412 (0.32 mm diameter) and N_2 carrier gas with a flow rate of approximately 3 mL min^{-1}. CO and CO_2
413 were analysed using a HP-PLOT/Q column (0.53 mm diameter) attached to a HP-5 column (0.32 mm
414 diameter) with a He carrier gas at an approximate flow rate of 2 mL min^{-1}. The GC oven temperature

was kept at 45 °C in both cases. Methane (2% CH_4 in N_2) was used as internal standard after calibration with different mixtures of known amounts of $H_2/D_2/CO/CO_2/N_2/CH_4$.

Mass spectrometry was carried out on a Hiden Analytical HPR-20 benchtop gas analysis system with custom-designed 8-way microflow capillary inlet to a HAL 101 RC electron impact quadrupolar mass spectrometer with a Faraday detector. The sample inlet was connected to the reactor headspace and the composition of gases with mass/charge ratios between 1 and 10 amu was analysed.

Treatment of data. All analytical measurements were performed in triplicate and are given as the unweighted mean ± standard deviation (σ). σ of a measured value was calculated using equation (1).

$$\sigma = \sqrt{\frac{\sum(x-\bar{x})^2}{n-1}} \qquad (1)$$

Where *n* is the number of repeated measurements, x is the value of a single measurement and $\bar{x}$ is the unweighted mean of the measurements. σ was increased to 5% of $\bar{x}$ in the event that the calculated σ was below this threshold.

The activity per weight of catalyst ($mol_{H_2}\ g_{cat.}^{-1}$ or $mol_{H_2}\ g_{CdS}^{-1}$) was calculated using equations (2) and (3) from the molar weight of the QD and co-catalyst (when added).

$$Activity\ (mol_{H_2}\ g_{cat.}^{-1}) = \frac{n_{H_2}}{4/3\pi r_{CdS}^3 N_a \rho_{CdS} n_{QD} + n_{co-cat.} m_{co-cat.}} \qquad (2)$$

$$Activity\ (mol_{H_2}\ g_{CdS}^{-1}) = \frac{n_{H_2}}{4/3\pi r_{CdS}^3 N_a \rho_{CdS} n_{QD}} \qquad (3)$$

Where n_{H_2} is the H_2 produced (mol), r_{CdS} is the radius of the QD (cm), ρ_{CdS} is the density of CdS (4.84 g cm^{-3}), N_a is Avogadro's number (mol^{-1}), n_{QD} is the number of moles of QD (mol), $n_{co\text{-}cat.}$ is the number of moles of added co-catalyst and $m_{co\text{-}cat.}$ is the mass of co-catalyst (taken as 232.54 g mol^{-1} for

434 $Co(BF_4)_2$). These values were divided by the irradiation time to calculate

435 $mol_{H_2}\ g_{cat.}^{-1}\ h^{-1}$ and $mol_{H_2}\ g_{CdS}^{-1}\ h^{-1}$.

436 **External quantum yield (EQY) determination.** 1 nmol of CdS-BF_4 in DMF was added to a quartz

437 cuvette (1 cm path length) and evacuated to dryness while stirring. 100 mg of cellulose and 2 mL of

438 10 M KOH were added and the cuvette was sealed with a rubber septum. The solution was purged

439 with N_2 containing 2% CH_4 for 10 min in the dark. Each sample was irradiated by a Xe lamp (LOT

440 LSH302) equipped with a monochromator (LOT MSH300) that was used to focus a single wavelength

441 of 430 nm (accurate to a full width at half maximum of 5 nm). The light intensity was adjusted to

442 between 700-800 mW cm^{-2}, which was measured using a power meter (ILT 1400, International Light

443 Technologies). The cuvette was irradiated across an area of 0.28 cm^2. The evolved headspace gas

444 was analysed by gas chromatography and the EQY (%) was calculated according to equation (4).

$$\mathrm{EQY} = 100\times\frac{2\times n\mathrm{H}_2\times N_A\times h\times c}{t_{irr}\times\lambda\times I\times A} \qquad (4)$$

445

446 Where $n\mathrm{H}_2$ is the amount of H_2 generated (mol), N_A is Avogadro's constant (mol^{-1}), h is Planck's

447 constant (J s), c is the speed of light (m s^{-1}), t_{irr} is the irradiation time (s), λ is the wavelength (m), I is

448 the light intensity (W m^{-2}) and A is the irradiated area of exposed to the light beam (m^2).

449 **Raman analysis.** Raman spectra were recorded using a confocal Raman spectrometer LabRam

450 (Horiba Jobin Yvon) equipped with a liquid nitrogen cooled Symphony CCD detector (Horiba Jobin

451 Yvon). A 514.73 nm line of an Ar ion laser (Coherent Innova 300c) was used as excitation

452 wavelength. 10 µM CdS-BF_4 QDs in water, 100 mM KOH and 10 M KOH were measured in a rotating

453 quartz cuvette. Accumulation time of the Raman spectra was 60 seconds. The laser power was set to

454 2.5 mW. The laser light was focused into the solution using a 20x objective (Nikon, 20x NA 0.5).

455 $Cd(OH)_2$ was obtained by slowly adding 1.5 mL of 1 M NaOH into 10 mL of a 0.1 M $CdSO_4$ solution.

The white precipitate was centrifuged and washed with Millipore water (ρ > 18.2 MΩ cm) three times.

Raman band-fitting analysis. Band fitting of the Raman spectra was employed to evaluate the band structures with low intensities arising at high KOH concentrations around the LO band at 305 cm^{-1}. For this, the spectra were first cut in the region from 225 cm^{-1} to 475 cm^{-1}. Then, the spectra of ligand-free CdS in water were fitted. As the LO band dominates the spectra, this band was fitted first using a Lorentzian band profile. The frequency is directly derived from the local maximum in the measured spectrum (*i.e.* 305 cm^{-1}). The band width was adjusted until the experimental band was properly accounted for, affording a width of 13 cm^{-1}, which is comparable to values reported in the literature. Small bands with frequencies around the LO frequency had to be included to enhance the match of generated and experimental spectrum (see Supplementary Figure 2b, green dashed lines). These bands do not necessary reflect real bands but may be a result of artefacts due to difficulties in baseline subtraction. The baseline at lower frequencies was dominated by a very strong polynomic increase of intensity towards the Rayleigh line, which made it difficult to properly estimate the baseline. As a result, the band width can be slightly inhomogeneous, which then requires inclusion of smaller bands around the middle frequency to achieve a match with convergence criteria of the fit. Importantly, the intensities of these bands are typically very low compared to the actual band. In this case, the integral intensities are smaller than 5 % and can therefore be neglected.

The spectra of ligand-free CdS in 10 M KOH were evaluated next using the bands already derived from the water spectra. To reconstruct the spectra properly more bands needed to be included, particularly on the low frequency side of the LO band. To account for the additional spectral contribution, the local intensity maxima were searched for and, at each frequency maximum, an additional Lorentz band was included with a pre-defined width of 20 cm^{-1}. Subsequently, the widths of these bands and their intensities were iteratively altered until the best convergence between overall fit and experimental spectrum was achieved (see Supplementary Figure 2c). This set of bands

481 was then used to fit the 0.1 M KOH spectra by allowing only the relative intensities of the bands to
482 change. The fit allowed a very good reconstruction of the spectra (see Supplementary Figure 2d).

483 **Zeta potential analysis.** A range of aqueous solutions with different pH values were made through
484 addition of various amounts of KOH or HCl to deionised water. The ionic strength of each solution
485 was kept constant at 0.5 M through addition of KCl. 2 nmol of CdS-BF_4 in DMF was injected into a vial
486 and dried. 1 mL of a given solution was added to the vial, the solution was sonicated for 20 min and
487 the pH was recorded. Zeta potential was measured in a disposable folded capillary cell on a Malvern
488 Zetasizer Nano Z zeta potential analyser.

489 **X-ray photoelectron spectroscopy**. 10 nmol of CdS-BF_4 in DMF was injected into a vial and the
490 solvent was removed while stirring. 2 mL of aqueous solution containing various [KOH] was added
491 and the solution was stirred for 5 min. The particles were isolated from solution through
492 centrifugation (10,000 rpm, 10 min), the supernatant was removed carefully and the resultant
493 yellow precipitate was transferred onto a gold-coated silicon substrate and dried. N.B., the dried
494 sample is very hygroscopic; as much supernatant as possible must be removed for the sample to dry
495 effectively.

496 **^{13}C-NMR spectroscopy of cellulose.** Prior to use, ^{13}C-cellulose (50 mg) was stirred for 20 min in 0.1 M
497 NaOH (10 mL) at 80 °C in air. The solid was collected by filtration, washed with water (500 mL) and
498 freeze dried, producing a fine white powder. A photoreactor was charged with CdS-BF_4 in DMF (1
499 nmol) and dried. ^{13}C-cellulose (10 mg) and 10 M NaOD in D_2O (1 mL) were added and the solution
500 was purged with N_2 (cont. 2% CH_4) and then irradiated for 3 days. Subsequently, the reaction
501 mixture was filtered through a hydrophilic syringe filter and a ^{13}C-NMR spectrum was taken of the
502 resultant solution.

503 To attain a spectrum of the insoluble cellulose, a photoreactor was charged with ^{13}C-cellulose (10
504 mg) and 10 M NaOD in D_2O (1.0 mL) either with or without CdS-BF_4 QDs (1 nmol). The resultant

solution was purged with N_2 and irradiated, as described above, for 12 hours. Subsequently, the reaction mixture was centrifuged (15 min, 12,000 rpm) and the solid residue was washed with water and freeze-dried to give a pale yellow powder. The yellow powder was added to an NMR tube containing $ZnCl_2$ (1.00 g), LiCl (200 mg) and D_2O (360 µL).[40] The mixture was degassed by three freeze-pump-thaw cycles, sealed and heated to 100 °C overnight. The resulting brown melt was cooled to room temperature before a ^{13}C-NMR spectrum was taken.

^{1}H-NMR spectroscopy of cellulose. A photoreactor was charged with CdS-BF_4 (2 nmol) and dried. α-cellulose (100 mg) and 10 M NaOD in D_2O (2 mL) were added and the solution was purged with N_2 (cont. 2% CH_4) and irradiated for 3 days. Subsequently, the reaction mixture was filtered through a hydrophilic syringe filter and a ^{1}H-NMR spectrum was taken of the resultant solution.

Transmission electron microscopy. CdS/CdO_x particles were prepared for TEM by adding CdS-BF_4 (1.5 nmol) to a vial and drying *in vacuo* while stirring. Aqueous KOH (0.2 mL, 10 M) was added and the resultant solution was sonicated for 5 min. The suspension was centrifuged at 10,000 rpm for 5 minutes and the supernatant was removed. The particles were re-suspended in diethyl ether (around 1 mL) and 10 µL of the suspension was loaded onto a Cu TEM (TAAB) grid and dried.

Fluorescence quantum yield determination. The absolute fluorescence quantum yield was determined using an Edinburgh Instruments Integrating Sphere Module (SC-30) on an Edinburgh Instruments FS5 spectrofluorometer according to equation (5) and previous reports.[53]

$$Fluorescence\ quantum\ yield\ (\%) = \frac{Photons\ emitted\ by\ sample}{Photons\ absorbed\ by\ sample} \times 100 \qquad (5)$$

To prepare the sample, CdS-BF_4 (4 nmol) was added to a vial and dried *in vacuo* while stirring. The QDs were then resuspended in 10 M KOH (3 mL) and stirred for 5 minutes. 2.5 mL of the CdS/CdO_x QD solution was added to a quartz cuvette (1 cm path length) to make the sample and a 2.5 mL solution of 10 M KOH in an equivalent cuvette was used as a reference. The number of photons absorbed by the sample (at 360 nm) was determined from the difference in the integrated spectra of

529 the excitation beams of the sample and reference solutions. The number of photons emitted by the
530 sample was calculated through the difference of the integrated fluorescence emission of the sample
531 between 440-550 nm and the reference. Fluorescence spectra analysis software (Fluoracle,
532 Quantum Yield Wizard, Edinburgh Instruments) then gave a value for the quantum yield.

533

534 The data that support the presented plots within this paper and other findings of this study are
535 available at the University of Cambridge data repository (add link before final publication).

536 **References**

537 1. U.S. Energy Information Administration. *Short-Term Energy and Summer Fuels Outlook*. (U.S.
538 Department of Energy, 2016).

539 2. Tertzakian, P. *A Thousand Barrels a Second: The Coming Oil Break Point and the Challenges*
540 *Facing an Energy Dependent World*. (McGraw-Hill Education, 2006).

541 3. Murray, J. & King, D. Oil's tipping point has passed. *Nature* **481,** 433–435 (2012).

542 4. IPCC, 2013. *Climate Change 2013: The Physical Science Basis. Contribution of Working Group I*
543 *to the Fifth Assessment Report of the Intergovernmental Panel on Climate Change*. (2013).

544 5. International Energy Agency. *Tracking Clean Energy Progress 2015 - Energy Technology*
545 *Perspectives 2015 Excerpt IEA Input to the Clean Energy Ministerial*. (2015).

546 6. Moret, S., Dyson, P. J. & Laurenczy, G. Direct synthesis of formic acid from carbon dioxide by
547 hydrogenation in acidic media. *Nat. Commun.* **5,** 4017 (2014).

548 7. Iulianelli, A., Liguori, S., Wilcox, J. & Basile, A. Advances on methane steam reforming to
549 produce hydrogen through membrane reactors technology: A review. *Catal. Rev.* **58,** 1–35
550 (2016).

551 8. US Department of Energy. *Multi-Year Research, Development, and Demonstration Plan - 3.1*

Hydrogen Production. *Multi-Year Research, Development, and Demonstration Plan* (Office of Energy Efficiency & Renewable Energy, 2015).

9. Rubin, E. M. Genomics of cellulosic biofuels. *Nature* **454,** 841–845 (2008).

10. Huber, G. W., Iborra, S. & Corma, A. Synthesis of Transportation Fuels from Biomass: Chemistry, Catalysts, and Engineering. *Chem. Rev.* **106,** 4044–4098 (2006).

11. Zinoviev, S. *et al.* Next-Generation Biofuels: Survey of Emerging Technologies and Sustainability Issues. *ChemSusChem* **3,** 1106–1133 (2010).

12. Puga, A. V. Photocatalytic production of hydrogen from biomass-derived feedstocks. *Coord. Chem. Rev.* **315,** 1–66 (2016).

13. Shimura, K. & Yoshida, H. Heterogeneous photocatalytic hydrogen production from water and biomass derivatives. *Energy Environ. Sci.* **4,** 2467–2481 (2011).

14. Xia, Q. *et al.* Direct hydrodeoxygenation of raw woody biomass into liquid alkanes. *Nat. Commun.* **7,** 11162 (2016).

15. Li, C., Zheng, M., Wang, A. & Zhang, T. One-pot catalytic hydrocracking of raw woody biomass into chemicals over supported carbide catalysts: simultaneous conversion of cellulose, hemicellulose and lignin. *Energy Environ. Sci.* **5,** 6383–6390 (2012).

16. Himmel, M. E. *et al.* Biomass Recalcitrance: Engineering Plants and Enzymes for Biofuels Production. *Science* **315,** 804–807 (2007).

17. Sun, Y. & Cheng, J. Hydrolysis of lignocellulosic materials for ethanol production: a review. *Bioresour. Technol.* **83,** 1–11 (2002).

18. Zhang, G. *et al.* Simultaneous cellulose conversion and hydrogen production assisted by cellulose decomposition under UV-light photocatalysis. *Chem. Commun.* **52,** 1673–1676 (2016).

575 19. Kawai, T. & Sakata, T. Conversion of carbohydrate into hydrogen fuel by a photocatalytic
576 process. *Nature* **286,** 474–476 (1980).

577 20. Speltini, A. *et al.* Sunlight-promoted photocatalytic hydrogen gas evolution from water-
578 suspended cellulose: a systematic study. *Photochem. Photobiol. Sci.* **13,** 1410–1419 (2014).

579 21. Yong, X. & Schoonen, M. A. A. The absolute energy positions of conduction and valence bands
580 of selected semiconducting minerals. *Am. Mineral.* **85,** 543–556 (2000).

581 22. Cao, S., Chen, Y., Wang, C.-J., Lv, X.-J. & Fu, W.-F. Spectacular photocatalytic hydrogen
582 evolution using metal-phosphide/CdS hybrid catalysts under sunlight irradiation. *Chem.*
583 *Commun.* **51,** 8708–8711 (2015).

584 23. Xu, Y. *et al.* Rational design of semiconductor-based photocatalysts for advanced
585 photocatalytic hydrogen production: the case of cadmium chalcogenides. *Inorg. Chem. Front.*
586 **3,** 591–615 (2016).

587 24. Budtova, T. & Navard, P. Cellulose in NaOH-water based solvents: a review. *Cellulose* **23,** 5–55
588 (2016).

589 25. Chang, C. M., Orchard, K. L., Martindale, B. C. M. & Reisner, E. Ligand removal from CdS
590 quantum dots for enhanced photocatalytic H_2 generation in pH neutral water. *J. Mater.*
591 *Chem. A* **4,** 2856–2862 (2016).

592 26. Spanhel, L., Haase, M., Weller, H. & Henglein, A. Photochemistry of Colloidal Semiconductors.
593 20. Surface Modification and Stability of Strong Luminescing CdS Particles. *J. Am. Chem. Soc.*
594 **109,** 5649–5655 (1987).

595 27. Moulder, J. F., Stickle, W. F., Sobol, P. E. & Bomben, K. D. *Handbook of X-ray Photoelectron*
596 *Spectroscopy: A Reference Book of Standard Spectra for Identification and Interpretation of*
597 *XPS Data*. (Physical Electronics, 1995).

598 28. Hammond, J. S., Gaarenstroom, S. W. & Winograd, N. X-ray Photoelectron Spectroscopic

599 Studies of Cadmium- and Silver-Oxygen Surfaces. *Anal. Chem.* **47,** 2193–2199 (1975).

600 29. Schreder, B. *et al.* Raman spectroscopy of II–VI semiconductor nanostructures: CdS quantum
601 dots. *J. Raman Spectrosc.* **34,** 100–103 (2003).

602 30. Kumar, S., Ojha, A. K. & Singh, R. K. Synthesis and Raman signature for the formation of
603 CdO/MnO2 (core/shell) nanostructures. *J. Raman Spectrosc.* **45,** 717–722 (2014).

604 31. Cuscó, R. *et al.* Raman scattering of cadmium oxide epilayers grown by metal-organic vapor
605 phase epitaxy. *J. Appl. Phys.* **107,** (2010).

606 32. Williams, R. & Labib, M. E. Zinc Sulfide Surface Chemistry: An Electrokinetic Study. *J. Colloid*
607 *Interface Sci.* **106,** 251–254 (1985).

608 33. Kuehnel, M. F., Wakerley, D. W., Orchard, K. L. & Reisner, E. Photocatalytic Formic Acid
609 Conversion on CdS Nanocrystals with Controllable Selectivity for H_2 or CO. *Angew. Chemie Int.*
610 *Ed.* **54,** 9627–9631 (2015).

611 34. Dworak, L. *et al.* Ultrafast Charge Separation at the CdSe/CdS Core/Shell Quantum
612 Dot/Methylviologen Interface: Implications for Nanocrystal Solar Cells. *J. Phys. Chem. C* **115,**
613 3949–3955 (2011).

614 35. Simon, T. *et al.* Redox shuttle mechanism enhances photocatalytic H_2 generation on Ni-
615 decorated CdS nanorods. *Nat. Mater.* **13,** 1013–1018 (2014).

616 36. Speltini, A. *et al.* Swine sewage as sacrificial biomass for photocatalytic hydrogen gas
617 production: Explorative study. *Int. J. Hydrogen Energy* **39,** 11433–11440 (2014).

618 37. Cai, J. & Zhang, L. Rapid Dissolution of Cellulose in LiOH/Urea and NaOH/Urea Aqueous
619 Solutions. *Macromol. Biosci.* **5,** 539–548 (2005).

620 38. Ramos, M. L., Caldeira, M. M. & Gil, V. M. S. NMR spectroscopy study of the complexation of
621 D-gluconic acid with tungsten(VI) and molybdenum(VI). *Carbohydr. Res.* **304,** 97–109 (1997).

622 39. Wolfel, R., Taccardi, N., Bosmann, A. & Wasserscheid, P. Selective catalytic conversion of
623 biobased carbohydrates to formic acid using molecular oxygen. *Green Chem.* **13,** 2759–2763
624 (2011).

625 40. Fischer, S., Leipner, H., Thümmler, K., Brendler, E. & Peters, J. Inorganic Molten Salts as
626 Solvents for Cellulose. *Cellulose* **10,** 227–236 (2003).

627 41. Zhao, J., Holmes, M. A. & Osterloh, F. E. Quantum Confinement Controls Photocatalysis: A
628 Free Energy Analysis for Photocatalytic Proton Reduction at CdSe Nanocrystals. *ACS Nano* **7,**
629 4316–4325 (2013).

630 42. Yang, J., Liu, H., Martens, W. N. & Frost, R. L. Synthesis and Characterization of Cobalt
631 Hydroxide, Cobalt Oxyhydroxide, and Cobalt Oxide Nanodiscs. *J. Phys. Chem. C* **114,** 111–119
632 (2010).

633 43. Wu, K. *et al.* Hole Removal Rate Limits Photodriven H_2 Generation Efficiency in CdS-Pt and
634 CdSe/CdS-Pt Semiconductor Nanorod–Metal Tip Heterostructures. *J. Am. Chem. Soc.* **136,**
635 7708–7716 (2014).

636 44. Kadam, S. R. *et al.* A green process for efficient lignin (biomass) degradation and hydrogen
637 production via water splitting using nanostructured C, N, S-doped ZnO under solar light. *RSC*
638 *Adv.* **4,** 60626–60635 (2014).

639 45. Li, C., Zhao, X., Wang, A., Huber, G. W. & Zhang, T. Catalytic Transformation of Lignin for the
640 Production of Chemicals and Fuels. *Chem. Rev.* **115,** 11559–11624 (2015).

641 46. Müller, U., Rätzsch, M., Schwanninger, M., Steiner, M. & Zöbl, H. Yellowing and IR-changes of
642 spruce wood as result of UV-irradiation. *J. Photochem. Photobiol. B: Biol.* **69,** 97–105 (2003).

643 47. Kumar, P., Barrett, D. M., Delwiche, M. J. & Stroeve, P. Methods for Pretreatment of
644 Lignocellulosic Biomass for Efficient Hydrolysis and Biofuel Production. *Ind. Eng. Chem. Res.*
645 **48,** 3713–3729 (2009).

646 48. Fang, X., Mark, G. & von Sonntag, C. OH radical formation by ultrasound in aqueous solutions
647 Part I: the chemistry underlying the terephthalate dosimeter. *Ultrason. Sonochem.* **3,** 57–63
648 (1996).

649 49. Goldstein, S., Aschengrau, D., Diamant, Y. & Rabani, J. Photolysis of Aqueous H_2O_2: Quantum
650 Yield and Applications for Polychromatic UV Actinometry in Photoreactors. *Environ. Sci.*
651 *Technol.* **41,** 7486–7490 (2007).

652 50. Awatani, T., Dobson, K. D., McQuillan, A. J., Ohtani, B. & Uosaki, K. In Situ Infrared
653 Spectroscopic Studies of Adsorption of Lactic Acid and Related Compounds on the TiO_2 and
654 CdS Semiconductor Photocatalyst Surfaces from Aqueous Solutions. *Chem. Lett.* **27,** 849–850
655 (1998).

656 51. Huang, L. *et al.* Dual Cocatalysts Loaded Type I CdS/ZnS Core/Shell Nanocrystals as Effective
657 and Stable Photocatalysts for H_2 Evolution. *J. Phys. Chem. C* **117,** 11584–11591 (2013).

658 52. Yu, W. W., Qu, L., Guo, W. & Peng, X. Experimental Determination of the Extinction
659 Coefficient of CdTe, CdSe, and CdS Nanocrystals. *Chem. Mater.* **15,** 2854–2860 (2003).

660 53. Suzuki, K. *et al.* Reevaluation of absolute luminescence quantum yields of standard solutions
661 using a spectrometer with an integrating sphere and a back-thinned CCD detector. *Phys.*
662 *Chem. Chem. Phys.* **11,** 9850–9860 (2009).

663

664 **Supplementary Information**

665 Supplementary Tables 1-10, Supplementary Figures 1-14 and Supplementary Video 1 are provided in
666 the Supplementary Information.

667

668 **Acknowledgements**

This work was supported by the Christian Doppler Research Association (Austrian Federal Ministry of Science, Research and Economy and the National Foundation for Research, Technology and Development), the OMV Group (to E.R.), the EPSRC (DTA studentship for D.W.W. and T.E.R), the Isaac Newton Trust, the German Research Foundation (to M.F.K.), the World Premier Institute Research Center Initiative (WPI), MEXT, Japan (to K.L.O.) and a Marie Curie Research fellowship (to K.H.L., GAN 701192 - VSHER). We would like to thank Mr Adam Brown (Cambridge, UK) for performing XPS measurements, Prof. Peter Hildebrandt (TU Berlin, German) for providing access to his laboratory to record Raman spectra and Dr Benjamin Martindale for proof-reading this manuscript.

Author contributions

D.W.W., M.F.K. and E.R. concieved the research. D.W.W. and M.F.K. performed photocatalysis and NMR experiments. D.W.W. and K.L.O. synthesised and characterized the QDs. K.L.O. executed TEM, XRD and the zeta potential analysis. K.H.L. carried out the Raman experiments. D.W.W. and T.E.R. carried out the fluorescence measurements. All authors analysed the data. D.W.W. wrote the manuscript. M.F.K., K.H.L. and E.R. added to the discussion and contributed to the preparation of the manuscript. E.R. supervised the work.

Author Information

*Correspondence and requests for materials should be addressed to reisner@ch.cam.ac.uk

END OF MANUSCRIPT